CARBON 66 (2014) 567–575

Available at www.sciencedirect.com

ScienceDirect

journal homepage: www.elsevier.com/locate/carbon

High and anisotropic thermal conductivity of body-centered tetragonal C_4 calculated using molecular dynamics

*Zhenqiang Ye, Bingyang Cao *, Zengyuan Guo*

Key Laboratory for Thermal Science and Power Engineering of Ministry of Education, Department of Engineering Mechanics, Tsinghua University, Beijing 100084, PR China

ARTICLE INFO

Article history:
Received 12 March 2013
Accepted 14 September 2013
Available online 20 September 2013

ABSTRACT

The thermal properties of body-centered tetragonal C_4 (bct-C_4), a new allotrope of carbon, were investigated using molecular dynamics (MD) simulations. The calculations gave a high and anisotropic thermal conductivity that is the first of its kind. The cross-plane thermal conductivity is 1209 W/(m K) at room temperature, which is even higher than that of diamond. The thermal conductivity decreases as the temperature increases from 80 to 400 K. The density of states of bct-C_4 was analyzed, which has a prominent peak at 36 THz. The relaxation times were calculated by fitting a heat flux autocorrelation function. The results showed that the acoustic phonons play the dominant role in the heat conduction, with a contribution of more than 99%. The relaxation times decrease with increasing temperature, as does the contribution of the acoustic phonons. Finally, the thermal conductivity based on lattice dynamics agreed well with that from the MD method, with which the group velocity and mean free path were deduced. This outstanding thermal property makes bct-C_4 a promising substitute for diamond, especially as thermal interface materials in microelectronic packaging.

1. Introduction

Carbon is one of the most important and fundamental elements on earth. Owing to the flexibility of the bond hybridizations, carbon can form various allotropes, such as diamond, graphite, and amorphous carbon [1]. The physical properties of these allotropes vary widely. For instance, diamond is the hardest substance in nature, but graphite is one of the softest [2]. Researchers are seeking to synthesize new carbon allotropes both theoretically and experimentally to find new materials with good electronic, magnetic, mechanical and thermal properties. Thus far, remarkable success has been achieved in developing carbon nanotubes (CNTs) [3] and graphene [4,5].

A recent study conducted by Omata et al. [6] discovered a new allotrope of carbon, body-centered tetragonal C_4 (bct-C_4), whose atomic structure consists of only C_4 square rings. They compressed various solid CNTs to different conditions using tight-binding molecular dynamics (MD) to obtain this peculiar bct-C_4 phase, when they compressed (10, 10) CNT lattices to 20 GPa.

Fig. 1 shows the crystal structure of bct-C_4 (Fig. 1a) compared to those of diamond (Fig. 1b) and graphite (Fig. 1c). The bct-C_4 structure consists entirely of sp3-hybridized carbon atoms, which is between the layered structure of graphite and the tetrahedral structure of diamond. The static structural parameters of bct-C_4 at 0 GPa are $a = 4.329$ Å, $c = 2.483$ Å, and two bond lengths, d_1 and d_2, of 1.562 and

* *Corresponding author:* Fax: +86 10 6279 4531.
E-mail address: caoby@tsinghua.edu.cn (B. Cao).
0008-6223/$ - see front matter
http://dx.doi.org/10.1016/j.carbon.2013.09.039

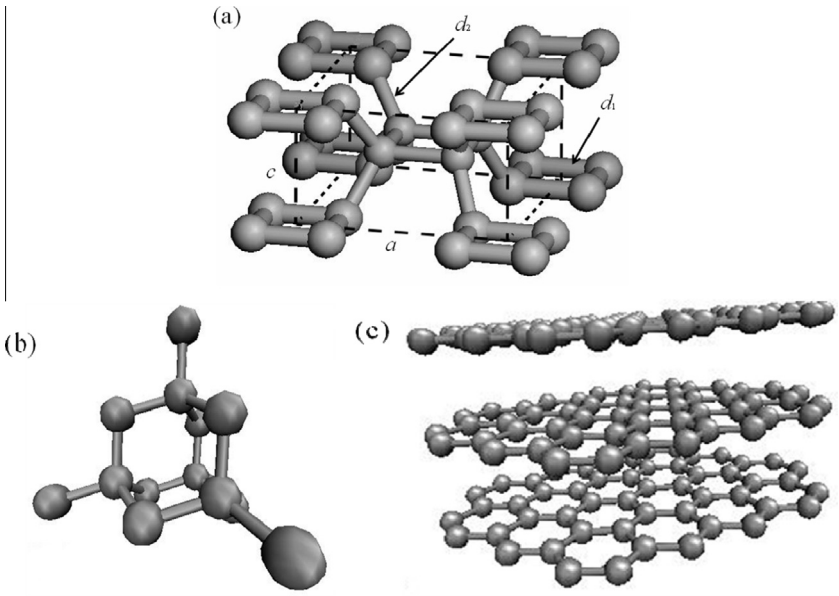

Fig. 1 – Crystal structures of bct-C_4 (a), diamond (b) and graphite (c).

1.506 Å [5]. The MD simulations revealed that bct-C_4 is a relatively stable phase in comparison to other carbon allotropes. It is more stable than the face-centered cubic solid C60 and as stable as (7, 0) and (8, 0) CNTs [7]. Xu et al. [2] investigated the mechanical properties and Vickers hardness of bct-C_4 based on first principle calculations and a microscopic hardness model. They found that bct-C_4 is mechanically stable at ambient conditions with the predicted Vickers hardness of 88 GPa, which is somewhat less rigid than that of diamond, but more rigid than most other materials. Hence, bct-C_4 is expected to be a potential superhard material. In addition, ab initio studies have indicated that bct-C_4 has outstanding shear strength, even larger than diamond [8]. The electronic, dielectric, optical, and vibrational properties of bct-C_4 have also been investigated [9–11]. The studies suggest that bct-C_4 is a stable phase with numerous useful features.

However, there are few reports about the thermal properties of bct-C_4. Heat removal is a crucial issue for the microelectronic industry, and the need for materials with excellent thermal conductivities is urgent in many industrial applications [12–14]. The exceptionally high thermal conductivities of CNTs and graphene have aroused much research interest in recent years [15–23]. Thus, the thermal conductivity of bct-C_4, a novel allotrope of carbon, is of great interest. Since the structure of bct-C_4 is like diamond, its thermal conductivity is expected to be as high as that of diamond.

The simulations show that the energy barrier from graphite to bct-C_4 is comparable to that to diamond [8]. Therefore, bct-C_4 could be an ideal substitute of diamond in some respects. For instance, diamond is widely noted as the thermal interface material in microelectronic packaging fields because of its high thermal conductivity and low dielectric constant [24,25], but it is rare and difficult to produce artificially. Since bct-C_4 has similar properties to diamond and it can be produced theoretically from graphite, it has potential for use in microelectronic packaging.

The aim of this study is to use MD simulations to investigate the thermal conductivity of bct-C_4. MD simulations have been proved to be very effective for studying thermophysical properties and have been widely used to investigate the thermal properties of carbon allotropes such as CNTs [15,16], graphene [18–22] and diamond [23]. Section 2 describes the theory and methodology and Section 3 provides results and discussion. The results describe the temperature dependence of the thermal conductivity of bct-C_4, which has a very high anisotropic thermal conductivity. The heat conduction mechanism is then analyzed based on the density of states (DOS) of phonons. The relaxation times of bct-C_4 are found by fitting the heat flux autocorrelation function (HAF). Finally, the thermal conductivity obtained from lattice dynamics is shown to agree well with the MD results, with the lattice dynamics results then used to deduce the phonon group velocity and the mean free path (MFP) of bct-C_4.

2. Theory and methodology

2.1. MD simulations of the thermal conductivity

The MD methods can be classified as equilibrium molecular dynamics (EMD) and nonequilibrium molecular dynamics (NEMD) methods. The EMD methods simulate the thermal conductivity of a system at equilibrium based on the fluctuation–dissipation theorem [15]. The NEMD methods establish a balance of the thermal transport by imposing a perturbation on a system, with the thermal conductivity obtained by solving the heat conduction equations. According to the method used to impose the perturbations, the NEMD methods can be classified as the homogeneous NEMD [26], reverse NEMD [27], uniform source-and-sink NEMD [28,29] and others. The NEMD methods run much faster than the EMD methods, but at the cost of less accuracy.

Since the EMD method is more precise, EMD simulations are used here to calculate the thermal conductivity of bct-C_4 based on the Green–Kubo formula [30]:

$$\lambda = \frac{1}{3VT^2k_B}\int_0^\infty \langle J(t)\cdot J(0)\rangle \, dt, \tag{1}$$

in which λ is the thermal conductivity, V is the system volume, T is the system temperature, k_B is Boltzmann's constant, t is the time, and $\langle\cdots\rangle$ denotes the ensemble average. $J(t)$ is the heat flux in the system at t moment and is defined as:

$$J(t) = \sum_i v_i E_i + \sum_i r_i \frac{dE_i}{dt}, \tag{2}$$

where r_i, v_i and E_i are the coordinate, velocity and total energy of atom i. The Brenner potential [31] has been widely used due to its superior performance in predicting the mechanical, chemical and thermal properties of hydrocarbon materials. Hence, the Brenner potential is used here to describe the interactions among the carbon atoms in bct-C_4. The Brenner potential can be written as:

$$\Phi = \sum_i \sum_{j>i} f(r_{ij})\left[V_R(r_{ij}) - \bar{b}_{ij}V_A(r_{ij})\right], \tag{3}$$

where Φ is the total potential entotal potential energy and V_R and V_A are the repulsive and attractive parts of the pairwise binding potential. V_R and V_A can be given by:

$$V_R(r_{ij}) = \frac{D}{S-1}\exp\left[-\beta\sqrt{2S}(r_{ij}-R_e)\right], \tag{4}$$

$$V_A(r_{ij}) = \frac{DS}{S-1}\exp\left[-\beta\sqrt{2/S}(r_{ij}-R_e)\right], \tag{5}$$

where D, S and β are interaction parameters, R_e is the atomic distance at zero potential, and $f(r_{ij})$ is the truncation function that explicitly restricts the interaction within the nearest neighbors. $f(r_{ij})$ is written as:

$$f(r_{ij}) = \begin{cases} 1, & r_{ij} < R^{(2)} \\ \frac{1}{2}\left[1+\cos\left(\frac{\pi(r_{ij}-R^{(1)})}{R^{(2)}-R^{(1)}}\right)\right], & R^{(1)} < r_{ij} < R^{(2)} \\ 0, & r_{ij} > R^{(2)} \end{cases}, \tag{6}$$

in which $R^{(1)}$ and $R^{(2)}$ are the critical values for chemical bond restructuring and breaking. The bond order parameter $\bar{b}_{ij}$ implicitly contains many-body information and is expressed by:

$$\bar{b}_{ij} = \frac{1}{2}(b_{ij}+b_{ji}), \tag{7}$$

$$b_{ij} = \left(1+\sum_{k(\neq i,j)} G(\theta_{ijk})f(r_{ik})\right)^{-\delta_c}, \tag{8}$$

$$G_c(\theta_{ijk}) = a_0\left[1+\frac{c_0^2}{d_0^2}-\frac{c_0^2}{d_0^2+(1+\cos\theta_{ijk})}\right]. \tag{9}$$

θ_{jik} stands for the included angle between carbon–carbon bonds, and δ_c, a_0, c_0, and d_0 are fitting parameters. Detailed parameters are provided in [31].

2.2. Thermal conductivity based on lattice dynamics

Phonons are quantized lattice vibrations which play a major role in heat conduction in semiconductors as well as dielectrics [32]. The Boltzmann transport equation (BTE) describes phonon transport in a succinct form. With the linear relaxation approximation [33], the BTE can be written as:

$$\frac{f-f_0}{\tau} = -v_g\nabla T\frac{\partial f}{\partial T}, \tag{10}$$

where f is the phonon distribution function, f_0 is the equilibrium distribution, v_g is the phonon group velocity, and τ is the relaxation time. Using the distribution function f, the net energy flux carried by the phonons can be described as:

$$Q = \frac{1}{V}\sum_p\sum_k h\nu f\cdot v_g(p,k), \tag{11}$$

in which Q denotes the net energy flux, ν_g is the phonon frequency, h is Planck constant, k is the wave vector, p is the polarization, and V is the system volume. Combining Eqs. (10) and (11) gives:

$$Q = -\sum_p\sum_k C(p,k)v_g^2(p,k)\tau(p,k)\cdot\nabla T, \tag{12}$$

where $C(p, k)$ represents the heat capacity per unit volume. Comparing Eq. (12) with Fourier's heat conduction law, $Q = -\lambda\nabla T$, gives the following expression for the thermal conductivity:

$$\lambda = \sum_p\sum_k C(p,k)v_g^2(p,k)\tau(p,k), \tag{13}$$

For convenience, each part can be replaced by an average value as:

$$\lambda = \frac{1}{3}Cv_g^2\tau = \frac{1}{3}Cv_g l, \tag{14}$$

in which l denotes the MFP.

2.3. Simulation details

The simulation region is a three-dimensional box with periodic boundary conditions. For each simulation, the system was initially brought to equilibrium using the *NVT* ensemble (constant number of atoms, *N*; constant volume, *V*; and constant temperature, *T*) for 200,000 steps to the designated temperature, with a time step of 0.5 fs. To study the size effect, the number of atoms was increased from 2000 to 16,000, and the system size increased from $5\times5\times10$ to $10\times10\times20$ unit cells (UCs). The system temperature was controlled by the Nose–Hoover thermostat [34]. Then, the system was allowed to evolve with the *NVE* ensemble (constant number of atoms, *N*; constant volume, *V*; and constant energy, *E*). The first 200,000 steps were used to relax the system, with the next 10,000,000 steps, i.e. t_{sum} = 5000 ps, used for recording the heat flux. The HAF was calculated based on the 10,000,000 sets of data. The Verlet algorithm [35] was used to numerically integrate the motion equations.

The ensemble average for the HAF was calculated using different initial times with an interval of t_{shift} = 0.1 ps and a sampling duration for the heat flux of t_{sample} = 1200 ps. Hence, the total number of samples is $(t_{sum}-t_{sample})/t_{shift}+1$ = 38,001. The phonon DOS was computed by taking the Fourier transform of the velocity autocorrelation function (VAF) [36]. The VAF is written as:

$$VAF(t) = \langle v(0)\cdot v(t)\rangle = \left\langle \frac{1}{N}\sum_{i=1} v_i(0)\cdot v_i(t)\right\rangle, \tag{15}$$

where $v_i(t)$ denotes the velocity of atom i at time t. The DOS expression is given by:

$$g(\omega) = \int \exp(-i\omega t)\mathrm{VAF}(t)\mathrm{d}t, \quad (16)$$

in which ω is the phonon angular frequency.

3. Results and discussion

3.1. Thermal conductivity

Fig. 2 shows the time-varying HAF and the convergence of the calculated thermal conductivity in terms of the integration of the HAF (the inset) at T = 300 K. The system had 16,000 atoms, and a size of $10 \times 10 \times 20$ UCs. The HAF rapidly converges in only 20 ps to 99% attenuation of the final value. The integration of the HAF increases rapidly at first, and then gradually becomes stable. This implies that the integration parameters, t_{sum}, t_{shift} and t_{sample}, are reasonable. The simulated thermal conductivity is sensitive to the initial conditions. In order to obtain reliable results, different cases were run with different initial conditions for each system temperature. The average of these cases gave the final results. As shown in Fig. 3, T = 300 K was used as a representative to illustrate the dependence of the calculated thermal conductivity on the case number. For ease of description, the normal to the tetragon is designed as the z axis, with the directions parallel to the tetragon as the x axis and the y axis. The plane parallel to the z axis is called cross-plane, while that constructed by the x and y axes is the in-plane. The thermal conductivities along x, y and z directions differ, which indicates that the thermal transport in bct-C_4 is anisotropic. The results in Fig. 3 show that a reliable result is obtained as the case number increases. The thermal conductivity in the x direction, λ_x, is approximately equal to that in the y direction, λ_y, but they are much less than that in the z direction, λ_z. The average thermal conductivity in the three directions, λ_{ave}, converges quickly. The bct-C_4 lattice structure is responsible for such behaviors. Firstly, λ_x should be theoretically equal to λ_y because of the symmetry of the lattices in the x–y plane. Secondly, the lattice bond length in the z direction is shorter than in the x and y directions. As mentioned earlier, the bond lengths are 1.562 and 1.506 Å. The shorter bond length denotes a larger bond energy, which leads to a higher thermal conductivity.

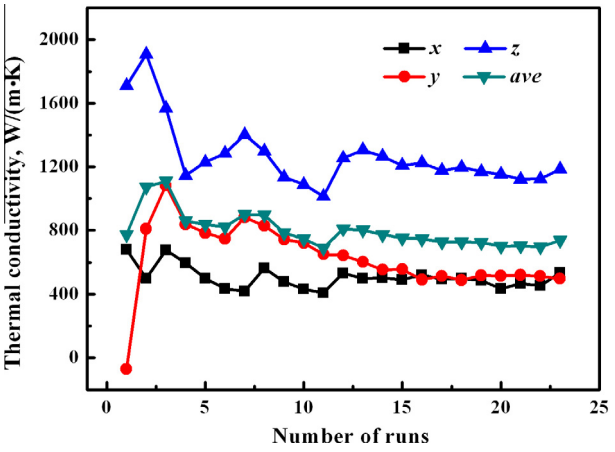

Fig. 3 – Dependence of the calculated thermal conductivity on the case number for T = 300 K. (A color version of this figure can be viewed online.)

The size effect on the calculated thermal conductivity is shown in Fig. 4. The system had atoms from 2000 to 16,000, with the system size from $5 \times 5 \times 10$ to $10 \times 10 \times 20$ UCs. The system temperature was 100 K, at which the size effect is more significant than that at higher temperatures due to its longer MFPs. The results show that the thermal conductivities along the three directions change only a tiny amount except for N = 2000. The simulation results are instable since there are only 2000 atoms. In general, the EMD method has very little size effect [29]. Hence, N = 16,000 is large enough to get reliable results and is used for the following results.

Fig. 5 presents the thermal conductivity of bct-C_4 from 80 K to 400 K. Several points should be noted in Fig. 5. Firstly, λ_x is approximately equal to λ_y and they both are less than λ_z at each temperature due to the different lattice structures.

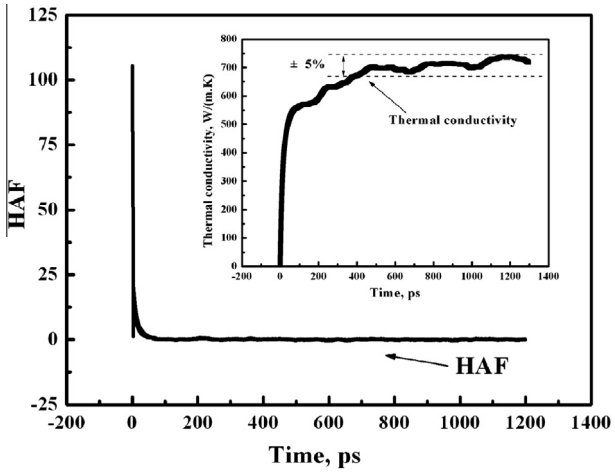

Fig. 2 – Time-varying HAF. The inset shows the converging thermal conductivity found by integrating HAF for T = 300 K.

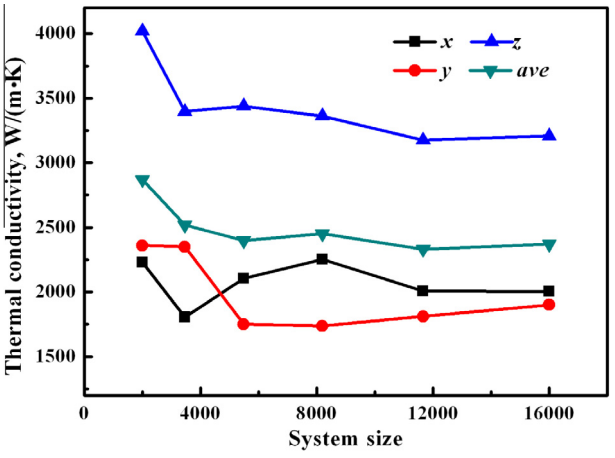

Fig. 4 – Size effect on the calculated thermal conductivity for T = 100 K. (A color version of this figure can be viewed online.)

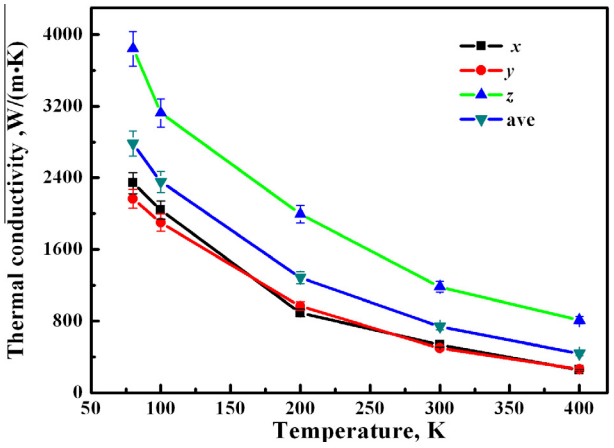

Fig. 5 – Temperature dependence of the thermal conductivity of bct-C_4. (A color version of this figure can be viewed online.)

Secondly, the thermal conductivity decreases with increasing temperature. In theory, the thermal conductivity should increase in the low temperatures and decrease in the high temperatures. Since the computations are less accurate at low temperatures [37], the thermal conductivity was only calculated above 80 K. The in-plane thermal conductivity, λ_{in}, decreases from 2254 to 256 W/(m K); the cross-plane thermal conductivity, λ_{cross}, decreases from 3843 to 802 W/(m K); and the average thermal conductivity decreases from 2710 to 436 W/(m K). At room temperature (300 K), λ_{in}, λ_{cross}, λ_{ave} are 502, 1209 and 738 W/(m K), respectively. The thermal conductivity of bct-C_4 will be compared to those of other carbon allotropes later. The downtrend of the thermal conductivity can be attributed to the decreasing phonon MFP. Eq. (14) indicates that the main factors impacting the thermal conductivity are the heat capacity and the MFP. At high temperatures, the heat capacity changes less than the MFP. As the temperature rises, more phonons are excited, which reduces the MFP.

The influence of the quantized phonons on the thermal conductivity can be illustrated by the DOS and weighted phonon DOS [38] (WDOS) of bct-C_4. The expression of the WDOS is:

$$\mathrm{WDOS} = g(\omega) f_0, \tag{17.a}$$

$$f_0 = \frac{1}{(e^{\hbar\omega/k_B T} - 1)}, \tag{17.b}$$

in which f_0 means the Bose–Einstein statistics [33]. The DOS of bct-C_4 at T = 200 K and 300 K are shown in Fig. 6. The DOS was calculated from the Fourier transform of the VAF. It shows that the tendencies of the two figures are almost the same and the peak is at about 36 THz, which agrees with the physical fact. Fig. 7 illustrates the WDOS of the bct-C_4 at 200 K and 300 K. Three points should be noted. First, few phonons are excited in the frequency region above 25 THz for both situations. Second, at 300 K, more phonons are excited than at 200 K. Third, the proportion of high-frequency (above 20 THz) at 300 K is about 0.2, while for 200 K is about 0.09. It means that there is a higher proportion of high-frequency phonons at 300 K, which has a negative effect on the thermal conductivity due to the Umklapp processes [39]. Hence, the main reason for the reduction of the thermal conductivity at high temperatures is that both the phonon occupation number and the proportion of high-frequency phonons increase with increasing temperature.

The thermal conductivities of bct-C_4 are compared with those of other carbon allotropes in Fig. 8. CNTs and graphene, as low-dimensional materials, have the highest thermal conductivity. The thermal conductivity of bct-C_4 is as high as diamond and much higher than those of polycrystalline graphite and amorphous carbon. The cross-plane thermal conductivity of bct-C_4 is larger than that of diamond. The bond length of diamond is 1.529 Å [23], while the bond length of bct-C_4 in the cross-plane is 1.506 Å. Hence, bct-C_4 has a higher cross-plane thermal conductivity. The in-plane thermal conductivity of bct-C_4 is slightly lower than that of diamond. Thus, bct-C_4 has a very high thermal conductivity, which suggests that it is a very promising material especially for thermal management of microelectronic devices.

To compare bct-C_4 with other allotropes further, Fig. 9a and b show the DOS of diamond and graphene, respectively.

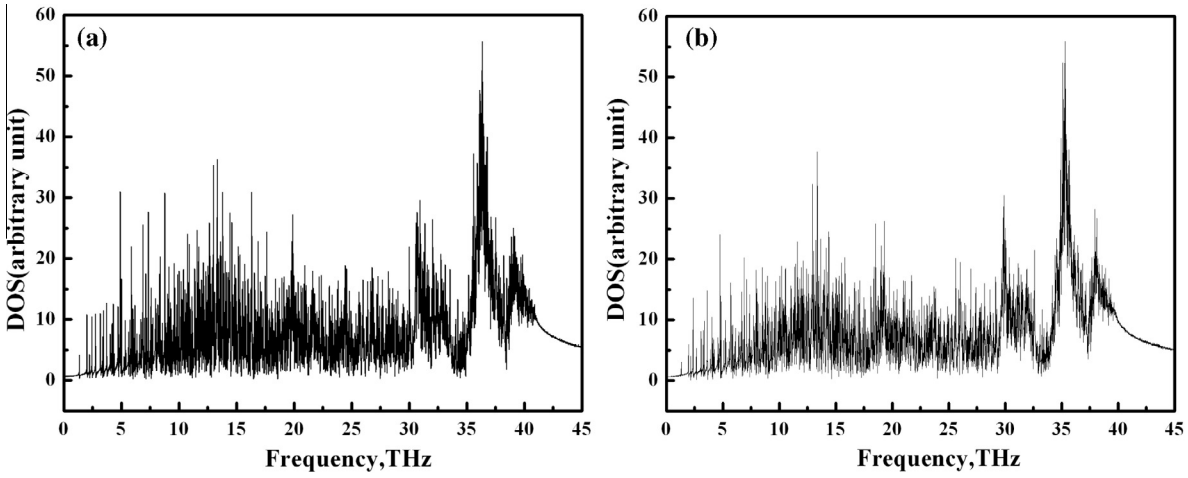

Fig. 6 – DOS of bct-C_4 at (a) T = 200 K and (b) 300 K.

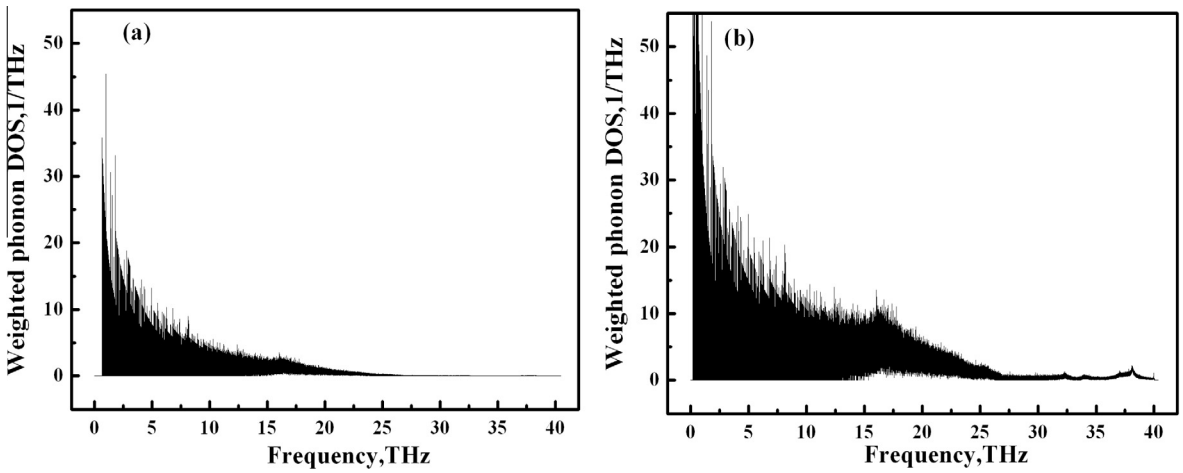

Fig. 7 – WDOS of bct-C_4 at (a) T = 200 K and (b) 300 K.

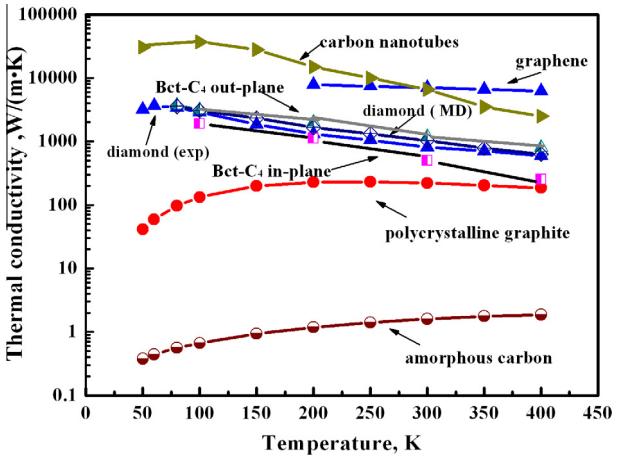

Fig. 8 – Thermal conductivities of carbon allotropes. The curve 'carbon nanotubes' is for isolated (10, 10) CNTs [16], which was calculated by MD simulations; 'graphene' is for suspended graphene flakes (100 μm) based on theoretical predictions [40]; 'diamond (MD)' was calculated in this work using the Brenner potential; 'diamond (exp)' was obtained by the experiments [41]; 'polycrystalline graphite' is for AGOT graphite [41] and 'amorphous' is for high-purity amorphous carbon [41]. (A color version of this figure can be viewed online.)

In diamond, the phonon spectrum has a prominent peak near 37 THz, and the high frequency states (above 20 THz) have a proportion of more than 70%. Comparing with Fig. 6, it can be found that the DOS of bct-C_4 is very similar with that of diamond. Both of them have a peak at about 36 THz and a high proportion of the high frequency states. But for graphene, it shows quite different features. First, the phonon spectrum of graphene has a wider frequency range and a higher maximum frequency than those of diamond and bct-C_4. Second, there are two peaks in high and low frequency region, respectively. The proportion of the high frequency states is as large as that of the low frequency states for graphene.

3.2. *Relaxation times of bct-C_4*

The phonon relaxation times can be extracted by fitting the HAF curve with an exponential function. Although the HAF curve at very short times (<20 fs) is not strictly exponential, this approximation does not have a significant effect on the final calculated thermal conductivity [23]. Phonon modes can be classified as low frequency acoustic modes and high frequency optical modes. These play different roles and make different contributions to the heat conduction. Hence, a double-exponential function is used to fit the HAF decay to identify the different effects of the two phonon modes. The double-exponential function is written as:

$$\mathrm{HAF}(t) = A_o \exp(-t/\tau_o) + A_a \exp(-t/\tau_a), \qquad t \geq 0, \tag{18}$$

where A denotes the fitting parameter and subscripts 'o' and 'a' stand for the optical and acoustic phonons [23]. The calculated HAF and the double-exponential function are shown in Fig. 10 for bct-C_4 at T = 300 K. The HAF decay can be divided into two stages. During the first stage, it decreases about 80% in only 0.04 ps, which reflects the contribution of the optical phonons. The acoustic phonons then play a significant role in the second stage. The contributions of the two phonon modes to the thermal conductivity are then related to the relaxation times. Integrating the double-exponential function gives the thermal conductivity as:

$$\lambda = \frac{1}{k_B T^2 V}(A_o\tau_o + A_a\tau_a). \tag{19}$$

The fitting results from 80 K to 400 K are listed in Table 1. At 300 K, τ_a and τ_o of bct-C_4 are 13.59 and 0.017 ps. Three important points can be noted in Table 1. The first is that the relaxation times decrease with increasing temperature due to the increasing phonon occupation. Second, the acoustic phonons have a greater effect on the heat conduction, with the acoustic phonons accounting for more than 99% of the heat conduction. Third, the contribution of the optical phonons to the thermal conductivity gradually increases with increasing temperature, with an increase of 0.73% as the temperature increases from 80 K to 400 K. This agrees with Goicochea et al. [42] who investigated the thermal properties of

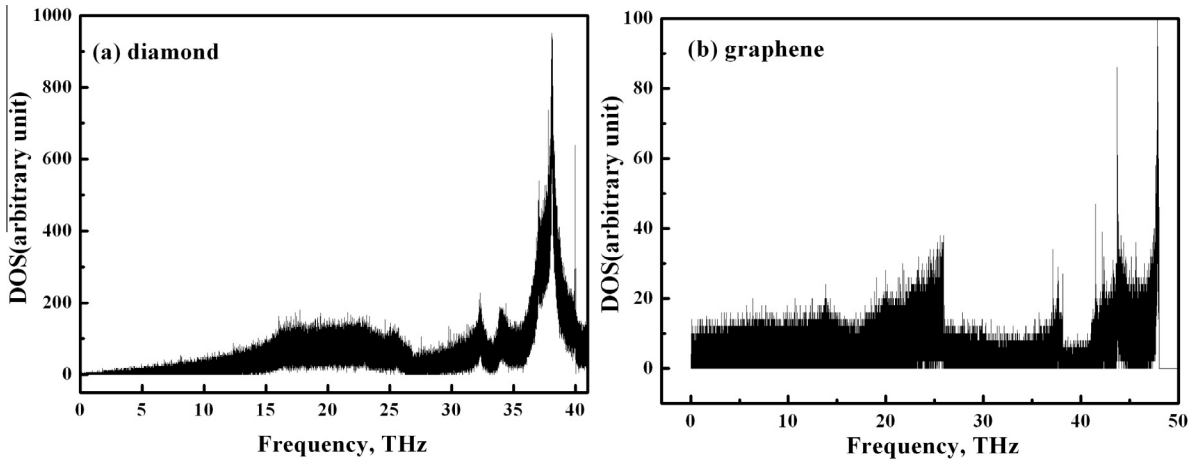

Fig. 9 – DOS of (a) diamond and (b) graphene for comparing with that of bct-C_4.

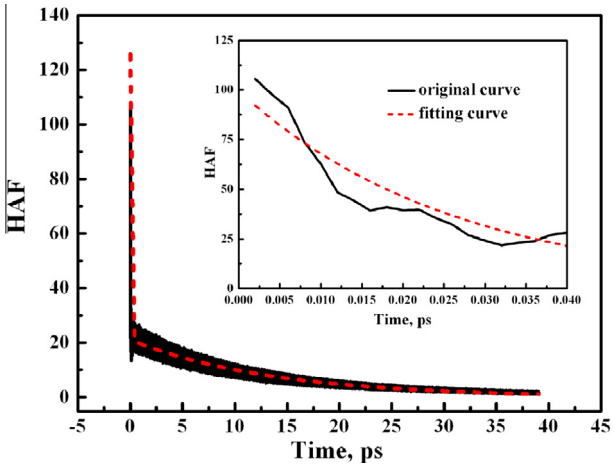

Fig. 10 – HAF and double-exponential function for T = 300 K. A partial view of short times is provided in the inset. (A color version of this figure can be viewed online.)

bulk silicon and found that the contribution of the optical phonons to the thermal conduction increased 0.87% as the temperature increased from 300 K to 1000 K.

3.3. *Lattice dynamics analyses*

The MD simulation results were validated by compared to Eq. (14) for the thermal conductivity of bct-C_4. Three key parameters need to be evaluated, the relaxation time, heat capacity and group velocity. Since the acoustic phonons have the dominant effect on the heat transfer, τ_a is used as the relaxation time, τ; thus ignoring the contribution from the optical phonons. The heat capacity using the Debye approximation [43] is expressed as:

$$C = 9Nk_B\left(\frac{T}{\Theta_D}\right)^3\int_0^{\Theta_D/T}\frac{e^{\xi}}{(e^{\xi}-1)^2}\xi^4 d\xi, \quad (20)$$

where Θ_D is the Debye temperature. Unfortunately, there is no reference value for the Debye temperature of bct-C_4 in the literatures. The Debye temperatures of diamond, graphene and CNTs are 1860, 2500 and 2300 K [44–46]. Thus, the De-

Table 1 – Curve-fit parameters for bct-C_4 from 80 K to 400 K.

T (K)	80	100	200	300	400
A_o	6.8453	10.962	45.85	117.8	390.36
τ_o (ps)	0.0321	0.0286	0.0247	0.017	0.00858
A_a	1.627	2.4867	9.6506	21.1	54.12
τ_a (ps)	57.463	39.814	22.304	13.59	6.36
λ_o (%)	0.23	0.32	0.52	0.69	0.96
λ_a (%)	99.77	99.68	99.48	99.31	99.04

Table 2 – Heat capacity, group velocity and MFP of bct-C_4 based on MD simulations and lattice dynamics analyses.

T (K)	80	100	200	300	400
C (J/(K m^3))	3.00×10^4	5.85×10^4	4.59×10^5	1.33×10^6	2.36×10^6
v_g (km/s)	68.71	55.06	21.22	11.30	9.33
MFP (μm)	3.95	2.19	0.473	0.153	0.059

bye temperature of bct-C_4 was assumed to be approximately 2100 K. The heat capacity at 300 K calculated using Eq. (21) is 1.33×10^6 J/(K m^3).The group velocity, v_g, is approximately equal to the sound velocity, i.e.:

$$v_g = \sqrt{\frac{B_0}{\rho}}, \tag{21}$$

in which B_0 is the bulk modulus and ρ is the density. At 300 K, B_0 is 418.2 GPa and ρ is 3.35×10^3 kg/m^3 [7], so v_g = 11.17 km/s. For T = 300 K, τ is 13.59 ps. Thus, the thermal conductivity of bct-C_4 at T = 300 K based on Eq. (8) is 750.58 W/(m K), which is very close to the MD simulation result, 738 W/(m K). Thus, the thermal conductivity based on lattice dynamics agrees with the MD simulation result.The group velocities, heat capacities and MFPs at other temperatures deduced from the calculated thermal conductivities of bct-C_4 are shown in Table 2. The group velocity decreases with increasing temperature. The MFP is as high as 3.95 μm at 80 K, but at room temperature, the MFP is only 0.153 μm, which is close to that of diamond, 0.174 μm [23].

4. Conclusions

The thermal properties of bct-C_4 were investigated using the EMD method. The results showed that bct-C_4 has a high anisotropic thermal conductivity. Analysis of the temperature dependence of the thermal conductivity of bct-C_4 showed that the thermal conductivity decreases at high temperatures. At room temperature, the average thermal conductivity is 738 W/(m K), with a cross-plane thermal conductivity of 1209 W/(m K), even higher than that of diamond. Analysis of the DOS and WDOS of bct-C_4 showed that the increases of the occupation and proportion of the high-frequency phonons are responsible for the decrease of the thermal conductivity. The DOS of bct-C_4 is similar to that of diamond with a peak of 36 THz in the high frequency region. The relaxation times of the acoustic and optical phonons were then extracted using a double-exponential function to fit the HAF. The optical relaxation time at 300 K is 0.017 ps while the acoustic relaxation time is 13.59 ps. The relaxation times decrease with increasing temperature due to the increasing phonon occupation. Further study showed that the acoustic phonons strongly dominant the heat conduction, with a contribution of about 99%. The contribution of the optical phonons increases only 0.73% as the temperature increases from 80 to 400 K. Finally, the thermal conductivity obtained using the lattice dynamics agrees well with the MD result. The group velocity and MFP were evaluated to be 11.3 km/s and 0.153 μm, for bct-C_4 at 300 K. In general, bct-C_4, a new allotrope of carbon, has excellent thermal properties, with an especially high cross-plane thermal conductivity. Combined with other outstanding features, such as high rigidity and good electronic and dielectric properties, bct-C_4 is a promising substitute for diamond in the future.

Acknowledgements

This work was financially supported by the National Natural Science Foundation of China (Nos. 51322603, 51321002 and 51136001), the Program for New Century Excellent Talents in University, the Tsinghua University Initiative Scientific Research Program, and the Tsinghua National Laboratory for Information Science and Technology (TNList) Cross-discipline Foundation.

REFERENCES

[1] Sheng XL, Yan QB, Ye F, Zheng QR, Su G. T-carbon: a novel carbon allotrope. Phys Rev Lett 2011;106(15):155703-1–4.
[2] Xu YH, Gao FM, Hao XF. Theoretical hardness and ideal tensile strength of bct-C_4. Phys Status Solidi RRL 2010;4(8):200–2.
[3] Iijima S. Helical microtubules of graphitic carbon. Nature 1991;354:56–8.
[4] Novoselov KS, Geim AK, Morozov SV, Jiang D, Katsnelson MI, Grigorieva IV, et al. Two-dimensional gas of massless Dirac fermions in graphene. Nature 2005;438(10):197–200.
[5] Lindsay L, Broido DA. Optimized Tersoff and Brenner empirical potential parameters for lattice dynamics and phonon thermal transport in carbon nanotubes and graphene. Phys Rev B 2010;81(20):205441-1–6.
[6] Omata Y, Yamagami Y, Tadano K, Miyake T, Saito S. Nanotube nanoscience: a molecular-dynamics study. Phys Rev E 2005;29(3):454–68.
[7] Umemoto K, Wentzcovitch RM, Saito S, Miyake T. Body-centered tetragonal C_4: a viable sp3 carbon allotrope. Phys Rev Lett 2010;104(12):125504-1–4.
[8] Zhou XF, Qian GR, Dong X, Zhang LX, Tian YJ, Wang HT. Ab initio study of the formation of transparent carbon under pressure. Phys Rev B 2010;82(13):134126-1–5.
[9] Lv ZL, You JH, Zhao YY, Wang H. Vibrational properties of body-centered tetragonal C_4. Commun Theor Phys 2011;55(3):513–8.
[10] Wei PY, Sun Y, Chen XQ, Li DZ, Li YY. Anisotropy in electronic, optical, and mechanical properties of superhard body-centered tetragonal C_4 phase of carbon. Appl Phys Lett 2010;97(6):061910-1–3.
[11] Tian YJ, Xu B, Zhao ZS. Microscopic theory of hardness and design of novel superhard crystals. Int J Refract Met Hard Mater 2012;33:93–106.
[12] Balandin AA. Thermal properties of graphene and nanostructured carbon materials. Nat Mater 2011;10(8):569–81.
[13] Cao BY, Kong J, Xu Y, Yung KL, Cai A. Polymer nanowire arrays with high thermal conductivity and superhydrophobicity fabricated by a nano-molding technique. Heat Transfer Eng 2013;34(2–3):131–9.
[14] Cao BY, Li YW, Kong J, Chen H, Xu Y, Yung KL, et al. High thermal conductivity of polyethylene nanowire arrays fabricated by an improved nanoporous template wetting technique. Polymer 2011;52(8):1711–5.
[15] Ruoff RS, Lorents DC. Mechanical and thermal properties of carbon nanotubes. Carbon 1995;33(7):925–30.
[16] Berber S, Kwon YK, Tománek D. Unusually high thermal conductivity of carbon nanotubes. Phys Rev Lett 2000;84(20):4613–6.
[17] Yang DJ, Zhang Q, Chen G, Yoon SF, Ahn J, Wang SG, et al. Thermal conductivity of multiwalled carbon nanotubes. Phys Rev B 2002;66(16):165440-1–6.
[18] Balandin AA, Ghosh S, Bao WZ, Calizo I, Teweldebrhan D, Miao F, et al. Superior thermal conductivity of single-layer graphene. Nano Lett 2008;8(3):902–7.
[19] Wei ZY, Ni ZH, Bi KD, Chen MH, Chen YF. In-plane lattice thermal conductivities of multilayer graphene films. Carbon 2011;49(8):2653–8.

[20] Chen SS, Wu QZ, Mishra C, Kang JY, Zhang HJ, Cho K, et al. Thermal conductivity of isotopically modified graphene. Nat Mater 2012;11(3):203–7.
[21] Pei QX, Sha ZD, Zhang YW. A theoretical analysis of the thermal conductivity of hydrogenated graphene. Carbon 2011;49(14):4752–9.
[22] Chien SK, Yang YT, Chen CK. Influence of chemisorption on the thermal conductivity of graphene nanoribbons. Carbon 2012;50(2):421–8.
[23] Che JW, Çağın T, Deng WQ, Goddard WA. Thermal conductivity of diamond and related materials from molecular dynamics simulations. J Chem Phys 2000;113(16):6888–900.
[24] Zweben C. Advances in composite materials for thermal management in electronic packaging. J Min Met Mater Soc 1998;50(6):47–51.
[25] Al-Sarawi SF, Abbott D, Franzon PD. A review of 3-D packaging technology. IEEE Trans Compon Packag Manuf Technol Part B 1998;21(1):2–14.
[26] Lukes JR, Zhong H. Thermal conductivity of individual single-wall carbon nanotubes. J Heat Transfer 2007;129(6):705–16.
[27] Müller-Plathe F. A simple nonequilibrium molecular-dynamics method for calculating the thermal-conductivity. J Chem Phys 1997;106(14):6082–5.
[28] Cao BY, Li YW. A uniform source-and-sink scheme for calculating thermal conductivity by nonequilibrium molecular dynamics. J Chem Phys 2010;133(2):024106-1–5.
[29] Cao BY, Dong RY. Nonequilibrium molecular dynamics simulation of shear viscosity by a uniform momentum source-and-sink scheme. J Comput Phys 2012;231(16):5306–16.
[30] Rowley RL, Painter MM. Diffusion and viscosity equations of state for a Lennard-Jones fluid obtained from molecular dynamics simulations. Int J Thermophys 1997;18(5):1109–21.
[31] Brenner DW. Empirical potential for hydrocarbons for use in simulating the chemical vapor deposition of diamond films. Phys Rev B 1990;42(15):9458–71.
[32] Chen G. Phonon heat conduction in nanostructures. Int J Therm Sci 2000;39(4):471–80.
[33] Henry AS, Chen G. Spectral phonon transport properties of silicon based on molecular dynamics simulations and lattice dynamics. J Comput Theor Nanosci 2008;5(2):141–52.
[34] Evans DJ, Holian BL. The Nose–Hoover thermostat. J Chem Phys 1985;83(8):4069–74.
[35] Auen MP, Tildesley DJ. Computer simulation of liquid. New York: Oxford University Press; 1987.
[36] Hu GJ, Cao BY. Molecular dynamics simulations of heat conduction in multi-walled carbon nanotubes. Mol Simul 2012;38(10):823–9.
[37] Turney JE, Landry ES, McGaughey AJH, Amon CH. Predicting phonon properties and thermal conductivity from anharmonic lattice dynamics calculations and molecular dynamics simulations. Phys Rev B 2009;79(6):064301-1–064301-12.
[38] Tohei T, Kuwabara A, Oba F, Tanaka I. Debye temperature and stiffness of carbon and boron nitride polymorphs from first principles calculations. Phys Rev B 2006;73(6):064304-1–6.
[39] Luckyanova MN, Garg J, Esfarjani K, Jandl A, Bulsara MT, Schmidt AJ, et al. Coherent phonon heat conduction in superlattices. Science 2012;338(61):936–9.
[40] Balandin AA, Ghosh S, Nika DL, Pokatilov EP. Thermal conduction in suspended graphene layers. Fullerenes Nanotubes Carbon Nanostruct 2010;18(4–6):474–86.
[41] Ho CY, Powell RW, Liley PE. Thermal conductivity of the elements: a comprehensive review. J Phys Chem Ref Data 1972;1(2):279–421.
[42] Goicochea JV, Madrid M, Amon C. Thermal properties for bulk silicon based on the determination of relaxation times using molecular dynamics. J Heat Transfer-Trans ASME 2010;132(1):012401-1–012401-11.
[43] Born M, Huang K. Dynamical theory of crystal lattices. Beijing: Peking University Press; 2011. p. 32–45 [in Chinese].
[44] Ekimov EA, Sidorov VA, Bauer ED, Mel'nik NN, Curro NJ, Thompson JD, et al. Superconductivity in diamond. Nature 2004;428(10):542–5.
[45] Maruyama S. A molecular dynamics simulation of heat conduction of a finite length single-walled carbon nanotube. Nanoscale Microscale Thermophys Eng 2003;7(1):41–50.
[46] Efetov DK, Kim P. Controlling electron–phonon interactions in graphene at ultrahigh carrier densities. Phys Rev Lett 2010;105(25):256805-1–4.